Journal of Physics B: Atomic, Molecular and Optical Physics

PAPER

Probing relaxation dynamics of a few strongly correlated bosons in a 1D triple well optical lattice

IOP Publishing Journal of Physics B: Atomic, Molecular and Optical Physics
J. Phys. B: At. Mol. Opt. Phys. **52** (2019) 215303 (10pp) https://doi.org/10.1088/1361-6455/ab2999

Probing relaxation dynamics of a few strongly correlated bosons in a 1D triple well optical lattice

S Bera[1], R Roy[1], A Gammal[2], B Chakrabarti[1,2,3,5] and B Chatterjee[4]

[1] Department of Physics, Presidency University, 86/1 College Street, Kolkata 700073, India
[2] Instituto de Física, Universidade de São Paulo, CEP 05508-090, São Paulo, Brazil
[3] The Abdus Salam International Center for Theoretical Physics, I34100 Trieste, Italy
[4] Department of Physics, Indian Institute of Technology-Kanpur, Kanpur 208016, India

E-mail: bchakra1@ictp.it

Received 21 February 2019, revised 29 May 2019
Accepted for publication 13 June 2019
Published 15 October 2019

Abstract

The relaxation process of a few strongly interacting bosons in a triple well optical lattice is studied from the first principle using the multiconfigurational time-dependent Hartree method for bosons. We report the contrasting response of the system under two independent quench processes: an interaction quench and a lattice depth quench. We analyze the evolution of the reduced one-body density matrix, two-body density and the Shannon information entropy for a wide range of lattice depth and interaction strength parameters. For the strong interaction quench, we observe a very fast relaxation to the steady state. In contrast, for the lattice depth quench, we observe collapse–revival dynamics in all the key measures. We also provide the best fitting formulas for relaxation and revival time which follow power law decay.

Keywords: interaction quench, lattice depth quench, information entropy

(Some figures may appear in colour only in the online journal)

1. Introduction

The non-equilibrium dynamics of isolated quantum systems have recently been triggered by remarkable experimental progress with ultracold trapped gases [1–10]. The simplest non-equilibrium process is quantum quench dynamics, where the system is driven out of equilibrium by abruptly changing any parameter of the Hamiltonian [11–24], while in a slow quench one parameter is slowly ramped up or down [25–28]. The onset of chaos and statistical relaxation are the most interesting research areas in non-equilibrium quantum physics. While the maximum entropy principle suggests which types of quantum systems should approach equilibrium, the mechanism of how the systems dynamically equilibrate, as well as the relaxation timescale and how it is related to the system parameters, are not well understood. The dynamics of entropy production and their connection with many-body correlation remain open problems. In this article, we explore the relaxation dynamics of interacting ultracold bosons in the optical lattice from a microscopic general quantum many-body perspective. The relaxation dynamics are simulated in the first principle by solving the time-dependent Schrödinger equation using the multiconfigurational time-dependent Hartree method for bosons (MCTDHB) [29–31].

We initially prepare the system in the superfluid (SF) phase and quench it to the Mott insulating (MI) phase through two independent quenches: i) quenching (instantaneously increasing) the interaction keeping the lattice depth constant, and ii) quenching the lattice depth keeping the interaction constant. We demonstrate the contrast between the two quenches by analyzing the one-body density matrix, two-body density, and entropy evolution.

For strong interaction quench, the system shows fast relaxation of all the calculated observables to the steady-state values. The relaxation time follows a power law decay as a function of the interaction strength and the Shannon

[5] Author to whom any correspondence should be addressed.

information entropy settles to a steady distribution. For the small interaction quench, the Shannon information entropy shows a periodic oscillation, and the time evolution of the reduced one-body density matrix exhibits collapse–revival dynamics. Whereas for lattice depth quench (with same excitation energy), we observe long-time collapse–revival dynamics in all measures, and the corresponding Shannon information entropy oscillates. The revival time exhibits a power law decay as a function of lattice depth. However, the response of the system for the lattice depth quench is slow. We repeat the simulation with a very strong lattice depth quench when the system is supplied with high excitation energy—we do not observe any signal of relaxation in the key measures in the present timescale of dynamics. However, the possibility of relaxation in very large timescale dynamics is not completely ruled out. We conclude that the key difference between the two setups lies in the fact that for the interaction quench, the system is pumped with the correlation energy, which is distributed as a two-body term in the Hamiltonian, while for the lattice depth quench, the system is pumped with potential energy which is distributed as a one-body term in the Hamiltonian. It is to be noted that the revivals for the lattice depth quench are known from Griener's experiment [5], whereas the fast relaxation for the interaction quench has neither been observed in an experiment nor been theoretically studied yet.

2. Setup

We consider N interacting bosons in a one-dimensional optical lattice. The Hamiltonian is given by

$$\hat{H} = \sum_{i=1}^{N}\left(-\frac{1}{2}\frac{\partial^2}{\partial x_i^2} + V_{OL}(x_i)\right) + \sum_{i<j}\hat{W}(x_i - x_j). \qquad (1)$$

Here V_{OL} represents the external lattice potential with periodic boundary condition modeled as $V_{OL}(x) = Vsin^2(kx)$, with V being the lattice depth and k the lattice wave vector. $\hat{W}(x_i - x_j) = \lambda\delta(x_i - x_j)$ represents the pairwise contact interaction where λ is the two-body interaction coupling strength between the bosons [32]. The Hamiltonian H is scaled in terms of the recoil energy $E_R = \hbar^2k^2/2m$, $\hbar = m = k = 1$, thus rendering all terms dimensionless. The time is expressed in units of $\frac{\hbar}{E_R}$ while distance is expressed as units of k^{-1}.

3. Method

We solve the time-dependent Schrödinger equation for N-interacting bosons, $\hat{H}\psi = i\frac{\partial\psi}{\partial t}$, using the MCTDHB method [29–31] as implemented in the MCTDH-X package [33–35]. This method has successfully been applied to extensively study various non-equilibrium bosonic systems [20–22, 31, 36–42].

In the MCTDHB method the many-body wave function is expanded as a linear combination of time-dependent permanents and the time-dependent weights as

$$|\psi(t)\rangle = \sum_{\vec{n}} C_{\vec{n}}(t)|\vec{n};\, t\rangle. \qquad (2)$$

The summation runs over all possible configurations $N_{conf} = \binom{N+M-1}{N}$. Note that the expansion coefficients $\{C_{\vec{n}}(t);\, \sum_i n_i = N\}$ *and* the orbitals $\{\phi_i(x,\, t)\}_{i=1}^{M}$ that build up the permanents are explicitly time dependent and variationally optimized quantities. In MCTDHB, $\vec{n} = (n_1,\, n_2,\, \ldots n_M)$ represent the occupations of the orbitals in a single configuration and $n_1 + n_2 + \ldots + n_M = N$, and M is the number of single particle functions that make up the permanents. Note that in the limit of $M \to \infty$, the set of permanents $\{|\vec{n};\, t\rangle\}$ span the whole Hilbert space and the expansion is exact. However, for practical calculation, we limit the size of the Hilbert space ensuring convergence in the measured quantities.

Let us remark on the issue of convergence of our simulation with MCTDHB. In the computation of the dynamics, the many-body wave function shows a strong fragmentation, i.e several natural orbitals have significant population. Thus the choice of the number of orbitals M is an important issue for our simulation, since an adequate number of orbitals is necessary to capture the correct physics. In general, the convergence can be ascertained by systematically increasing the number of orbitals and observing no change in the calculated quantities such as energy, relaxation time and entropy production. Additionally, the convergence is further assured when the occupation of the highest orbital is negligible. We find that for the interaction quench, $M = 18$ orbitals are required to achieve convergence and any further increase of M does not produce any change in the computed quantities. On the other hand, for the lattice depth quench, $M = 6$ is sufficient to achieve convergence. The stark difference can be understood by the fact that in the interaction quench, the system is highly correlated and the eigenstates contributing to the dynamics pertain to the (almost) completely available Hilbert space. In the lattice depth quench, although the many-body wave function is fragmented, the system is less correlated, and the contributing eigenstates cover only a small portion of the Hilbert space.

In our simulation, we analyze the following quantities:

(i) The first order reduced density matrix (RDM),

$$\rho^{(1)}(x'|x;\, t) = N\int dx_2 dx_3 \ \ldots\ , dx_N\, \psi^*(x',\, x_2,\, \ldots,\, x_N;\, t)\, \psi(x,\, x_2,\, \ldots,\, x_N;\, t). \qquad (3)$$

(ii) Natural occupations n_i which are the eigenvalues of $\rho^{(1)}$.

(iii) Two-body densities,

$$\rho^{(2)}(x_1',\, x_2'|x_1,\, x_2;\, t) = N(N-1)\int dx_3 dx_4\, \ldots . dx_N\, \psi^*(x_1',\, x_2',\, x_3,\, \ldots,\, x_N;\, t)\psi(x_1,\, x_2,\ldots x_N;\, t). \qquad (4)$$

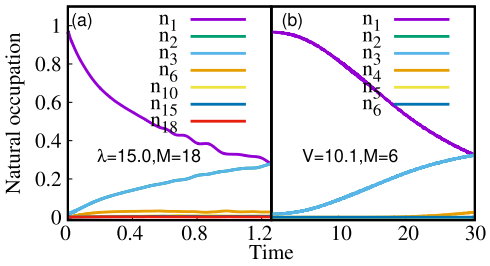

Figure 1. (a) Natural occupations as a function of time for interaction quench to $\lambda = 15.0$. Computation is done with $M = 18$ orbitals. The initial condensed *SF* phase fragments with time and the lowest three natural orbitals are occupied. At time $t = 1.25$, the system becomes a fully fragmented *MI* phase with ≈30% occupation of the lowest three orbitals. (b) Natural-orbital occupations as a function of time for the lattice-depth quench to $V = 10.1$. Computation is completed with $M = 6$ orbitals. The initial *SF* phase fragments with time and all three natural orbitals are occupied. At time $t = 31.0$, the system becomes a fully fragmented *MI* phase with almost 30% natural occupation in three orbitals. In both the occupation plots shown above n_2 and n_3 overlap with each other due to translational invariance. The contribution from all the other higher orbitals are negligible and they almost overlap. All quantities are dimensionless.

Its diagonal form is $\rho^{(2)}(x_1, x_2; t) \equiv \rho^{(2)}(x_1' = x_1, x_2' = x_2|x_1, x_2; t)$ which measures the probability to find two particles simultaneously at positions x_1 and x_2 at time t.

(iv) Many-body Shannon information entropy [41, 43],

$$S(t) = -\sum_i \bar{n}_i(t)[\ln \bar{n}_i(t)], \bar{n}_i = \frac{n_i}{N}. \quad (5)$$

4. Result

4.1. Interaction quench

Our setup consists of $N = 3$ bosons in a one-dimensional triple well ($S = 3$) optical lattice with periodic boundary condition. For the interaction quench, the interaction strength λ is changed suddenly keeping the depth of the lattice V fixed. To achieve the $SF \rightarrow MI$ transition with the interaction quench, the ground state is prepared for depth $V = 3.0$ and $\lambda = 0.1$ initially. Then, keeping V fixed, λ is changed instantaneously to $\lambda = 15.0$. This corresponds to pumping the system with energy $E = 4.89$ through the two-body interaction term in the Hamiltonian.

In our small ensemble of few particle systems, the notion of quantum phases cannot be applied rigorously. Rather, we obtain many-body states which are the few-body analog to the thermodynamic phases. In this paper, for the sake of simplicity and clarity of explanation, we term these few-body states as phases.

In figure 1(a), we plot natural orbital occupations n_i as a function of time. Initially, at $t = 0$ only the first natural orbital contributes, which corresponds to the *SF* phase, and the many-body wave function is condensed, equivalent to the mean-field state, represented as $|3, 0, \ldots, 0\rangle$, where the number denotes the population of the corresponding orbitals. With increasing time, fragmentation occurs, and at $t = 1.25$ the lowest three orbitals exhibit population of almost 30%, which is nearly three-fold fragmentation. This three-fold fragmented state $|1, 1, 1, 0, \ldots, 0\rangle$ corresponds to the *MI* state. Thus at time $t = 1.25$, the system makes a transition from the condensed *SF* to fragmented *MI* phase. The time evolution of natural orbitals at a higher time and the associated discussions are presented in appendix A for convenience.

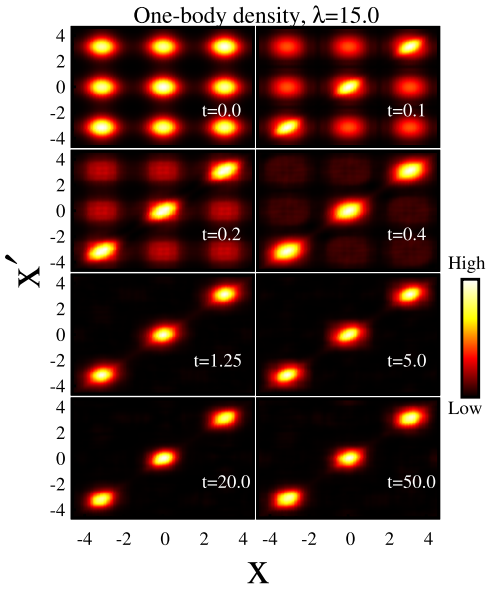

Figure 2. Time evolution of the reduced one-body density matrix $|\rho^{(1)}(x', x)|^2$ for interaction quench $\lambda = 15.0$. We observe very fast relaxation to the *MI* phase (see text). All the quantities are dimensionless.

Figure 2 shows the reduced one-body density matrix $|\rho^{(1)}(x', x)|^2$ at different times. Initially, at $t = 0$, we observe a uniform distribution of maxima showing that the initial state (which is *SF*) displays both intra-well as well as inter-well phase coherence. As time t increases, the off-diagonal maxima fade out and the diagonal contributions become more pronounced. At time $t = 1.25$, which corresponds to the equivalent *MI* phase, only the diagonal maxima are observed with a complete absence of off-diagonal contributions showing a complete absence of phase-coherence. From long timescale dynamics, we do not observe any revival of coherence and can conclude that the system relaxes. Thus figures 1(a) and 2 jointly conclude that $t = 1.25$ is the required time for the system to enter into the *MI* phase. The complete extinction of off-diagonal correlation after a long period of time also supports that the *MI* phase is retained. However, at the intermediate time, we found that the system tries to build up some inter-well coherence; this is discussed in appendix A.

The corresponding two-body density $\rho^{(2)}(x_1, x_2)$ is shown in figure 3. At $t = 0.1$, the diagonal maxima show a reduction in amplitude compared to the off-diagonal maxima. However, at time $t = 1.25$, an equal distribution per site is achieved, although the diagonal does not extinguish completely. With

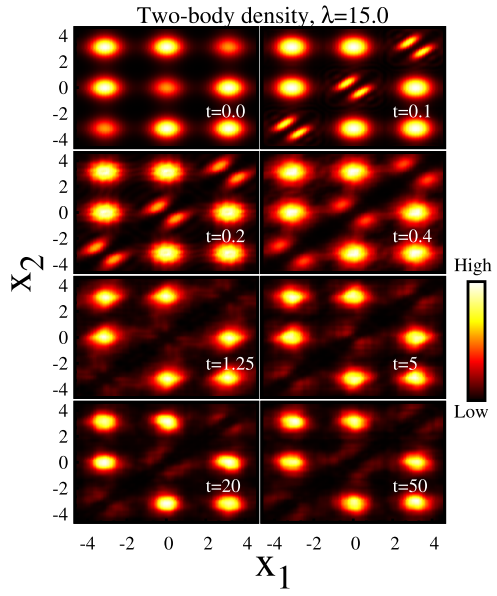

Figure 3. Time evolution of the two-body density $\rho^{(2)}(x_1, x_2)$ for interaction quench $\lambda = 15.0$. All the quantities are dimensionless.

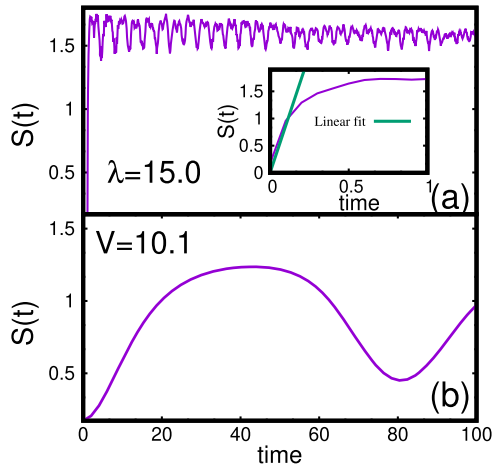

Figure 4. (a) Time evolution of Shannon information entropy $S(t)$ for interaction quench $\lambda = 15.0$. The sharp linear increase followed by saturation signify that the system relaxes to the maximum entropy state. The inset presents the sharp linear increase fitted with the analytical formula (see text) for a short period of time. (b) Time evolution of Shannon information entropy $S(t)$ for lattice-depth quench $V = 10.1$. The entropy exhibits periodic oscillation and the possibility of relaxation is ruled out. All the quantities are dimensionless.

increasing time, the diagonal contributions fade out, and complete depletion of the diagonal is achieved at a much longer time which is sustained for a long time further demonstrating the relaxation process.

The corresponding Shannon information entropy as a function of time is shown in figure 4(a). We observe a generic linear increase at a shorter time followed by saturation (see inset of figure 4(a)). The sharp linear increase in $S(t)$ is attributed to an exponential increase in the time-dependent natural occupation contributing to the dynamics and is described as $S(t) = \Gamma\, t\, \ln P$, where Γ is determined by the decay probability to stay in the initial ground state and P is

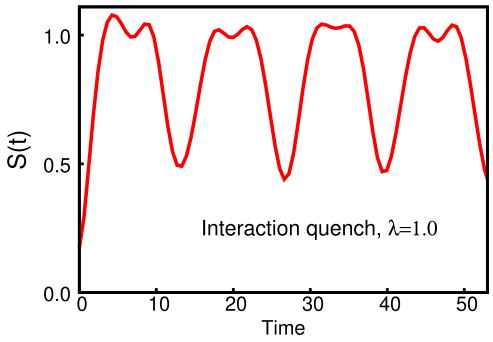

Figure 5. Dynamics of Shannon entropy $S(t)$ for interaction quench $\lambda = 1.0$. The entropy shows periodic oscillation. All the quantities are dimensionless.

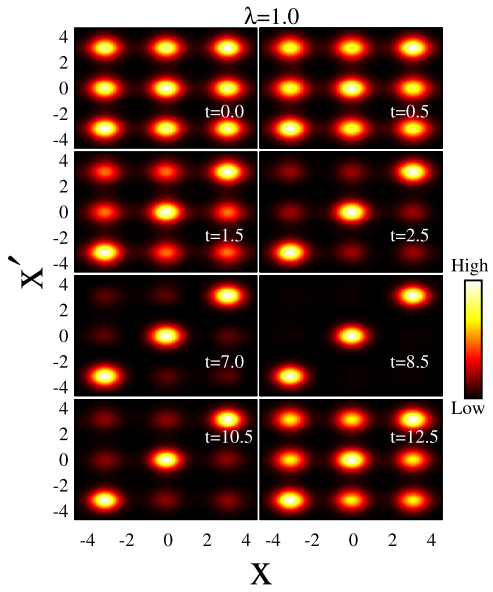

Figure 6. Time evolution of the reduced one-body density matrix $|\rho^{(1)}(x', x)|^2$ for interaction quench $\lambda = 1.0$. Collapses and revivals demonstrate how the matter-wave field dephases and rephases periodically during its time evolution. The system does not relax. All the quantities are dimensionless.

the number of many-body states involved in the dynamics [44]. The saturation of $S(t)$ happens at $t = 1.25$ due to the complete occupation of the available finite sized Hilbert space.

It is also instructive to report the dynamics for small interaction strength quench $\lambda = 1.0$. Figures 5 and 6 report the entropy dynamics and time evolution of the reduced one-body density matrix respectively for small interaction strength quench $\lambda = 1.0$. The amount of excitation energy received is very small, which induces a small perturbation to the system. The variation of entropy shows a periodic oscillation [45]. The corresponding time evolution in the one-body density matrix (figure 6) shows the system clearly enters into the *MI* phase at time $t = 8.5$, which is characterized by complete extinction of off-diagonal correlation; however, it revives at time $t = 12.5$, which corresponds to the time of occurrence of the first deep kink in the entropy production (figure 5). The corresponding two-body density (not shown here) distinctly

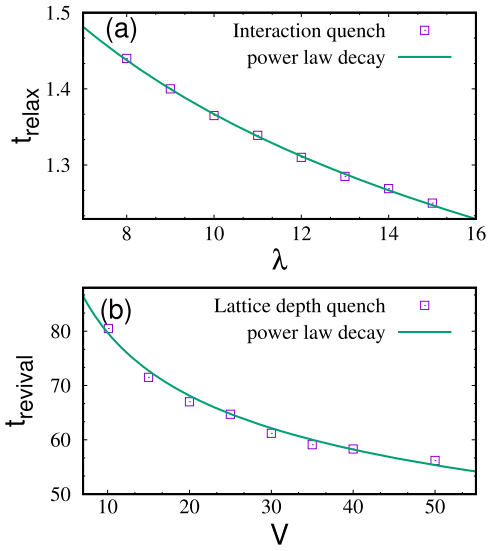

Figure 7. (a) Relaxation time t_{relax} for interaction quench. The curve shows the power law decay. The best fit formula is $t_{relax} = 2.3\ \lambda^{-0.23}$. (b) Revival time $t_{revival}$ for lattice-depth quench. The curve shows power law decay. The best fit formula is $t_{revival} = 134.5\ V^{-0.23}$. All the quantities are dimensionless.

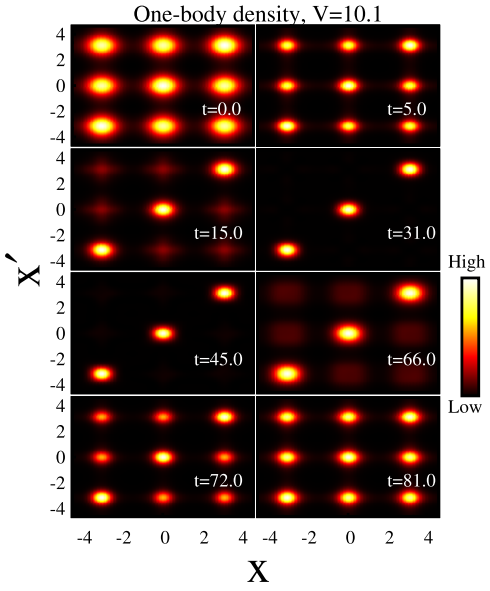

Figure 8. Time evolution of the reduced one-body density matrix $|\rho^{(1)}(x', x)|^2$ for lattice-depth quench $V = 10.1$. The system exhibits revival in the long time dynamics. All the quantities are dimensionless.

exhibits the revival phenomena. In our numerical simulation, we observe that for a strong interaction quench, the system relaxes to a steady state. For a weak interaction quench, the system shows collapse–revival for long timescales, which is displayed in the periodic oscillation of the entropy in sharp contrast with the generic linear increase followed by saturation for a strong interaction.

Figure 1(a) shows $t = 1.25$ is the required time for the system to enter the *MI* phase and this is also the same time when the off-diagonal correlation is completely lost. However, figures A1 and A2 of appendix A, for the intermediate time zone, show that the first orbital builds up population more than 33% and some faded off-diagonal coherence is also built up accordingly. However, the *SF* phase never turns back. The small intermediate kinks in the entropy plot in figure 4(a) also support the same observation. Thus we strictly follow the definition of t_{relax} in three ways: a) the system enters to the fully fragmented *MI* state for the first time; (b) one-body diagonal correlation is only maintained; (c) the system relaxes to a steady state. In figure 7(a) we plot t_{relax} for different (strong) λ quenches and observe a power law decay as $t_{relax} = 2.3\ \lambda^{-0.23}$. Note that in the tight-binding approximation (equation (C.2) and equation (C.3) of appendix C), the interaction energy U scales as a linear function of interaction strength λ and with $\frac{1}{4}$ power of the lattice depth. Whereas hopping term J depends solely on the lattice depth V in a complicated way. Thus one-to-one correspondence between (U, J) and (λ, V) does not hold. In figure C3(a) therefore we plot t_{relax} as a function of $\frac{U}{J}$, which also exhibits the power law decay.

4.2. Lattice depth quench

For the lattice depth quench, we prepare an identical initial state as for the interaction quench ($\lambda = 0.1$, $V = 3.0$) and instantaneously increase the lattice depth to $V = 10.1$, keeping λ fixed. The values are chosen such that the system is pumped with the same excitation energy $E = 4.89$ as the $\lambda = 15.0$ interaction quench. However, as the pumped energy is now distributed as the one-body term in the Hamiltonian, the system responds differently in the dynamics. In figure 1(b), we plot the evolution of natural occupation. The initial *SF* state becomes fragmented and enters the fragmented *MI* state for the first time at $t = 31.0$ which is significantly larger than $t = 1.25$. This significantly slower $SF \rightarrow MI$ transition, i.e. a larger characteristic time to reach the *MI* phase which distinguishes the lattice depth quench from the interaction quench.

The corresponding reduced one-body density matrix is presented in figure 8 which clearly exhibits long-time collapse–revival dynamics reminiscent of those observed in Greiner's experiment [5, 6]. The phase coherence revives at $t = 81.0$ which corresponds to the *SF* phase. The time evolution of the two-body density is shown in figure 9. The diagonal maxima are reduced with time but are completely depleted and revive over a long timescale.

The corresponding Shannon entropy evolution, shown in figure 4(b), also exhibits the periodic oscillation. The absence of a generic linear increase and saturation demonstrate that the system does not relax. To check the possibility of relaxation for very strong lattice depth quench, we repeat the simulation for a very deep lattice depth quench when the system is pumped with huge excitation energy, but we do not find any signature of relaxation; the system always revives and the revival time decreases with an increase in the lattice depth.

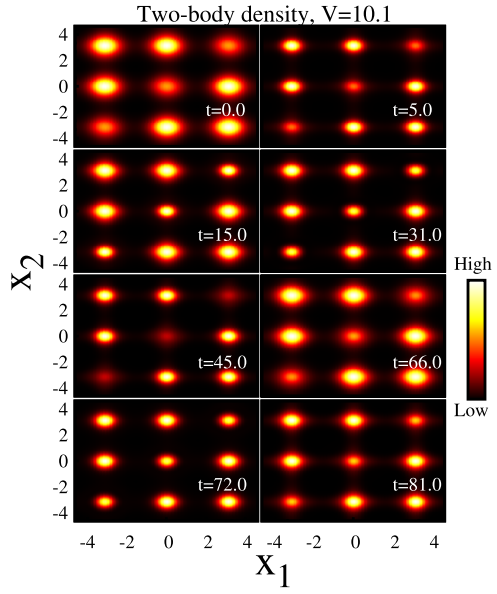

Figure 9. Time evolution of the two-body density $\rho^{(2)}(x_1, x_2)$ for lattice-depth quench $V = 10.1$. All the quantities are dimensionless.

However, if we increase the computation time the system may eventually relax. From figure 4(b), we observe a broad maxima from $t = 31.0$ to $t = 56.0$, which signifies that the system retains in the *MI* phase for this duration of time and then revives to its minimum entropy state at time $t = 81.0$, which is the same as that reported in figure 8 where the *SF* phase is revived. Thus $t = 81.0$ can be taken as the revival time for $V = 10.1$ lattice depth quench. We define the revival time ($t_{revival}$) as the time when the system revives global phase coherence in one-body density, and the corresponding entropy reaches its minimum. In figure 7(b), we plot $t_{revival}$ as a function of the lattice depth, which follows a power law decay fitted as $t_{revival} = 134.5\ V^{-0.23}$. The qualitative nature of variation of $t_{revival}$ with the lattice depth resembles the same nature as that observed in Greiner's experiment [5, 6]. In figure C3(b), we plot $t_{revival}$ as a function of $\frac{U}{J}$, which clearly exhibits the slow response of the system in the lattice depth quench. The explanation is as follows. For both the interaction and lattice depth quench the system receives the same amount of energy, however the dynamical response of the system is determined by how the received energy is distributed by the system. It is understandable that for the interaction quench, the received energy is quickly distributed through the two-body interaction term of the Hamiltonian, thus the response time which is characterized by the relaxation time in our computation exhibits falls quickly with the $\frac{U}{J}$ ratio. Whereas for the lattice depth quench, the Hamiltonian distributes the received energy through the one-body potential, it is exhibited by slow response of the system, and the revival time weakly depends on the $\frac{U}{J}$ ratio.

Our present simulation is based on the simplest problem of three bosons in three wells, which is the building block of many-body physics. The immediate question in this direction is to investigate the finite size effect, keeping the density fixed. We report our results for $N = 5$ bosons in $S = 5$ wells in appendix B. For the completion of our work, we also present a connection between the Bose–Hubbard physics and the many-body physics in appendix C.

5. Conclusion

In this paper, we have studied the quench dynamics of 1D interacting bosons in an optical lattice from the first principle general quantum many-body perspective using the MCTDHB method, covering both the significantly strong interactions and the shallow optical lattice. We observe that the dynamics of the two different quenches show significantly different behavior. For the strong interaction quench, the system enters the *MI* phase over a small timescale and relaxes to that maximum entropy state. The relaxation process is observed through the time evolution of the natural occupations, entropy evolution, and the reduced density matrices. The relaxation time follows a power law decay with respect to the interaction strength. In contrast, for the lattice depth quench with the same excitation energy, the *MI* phase is reached over a very long timescale, significantly larger than that of the interaction quench. For the lattice depth quench, the system does not relax and exhibits collapse–revival dynamics over a long timescale, which is revealed in all the computed measures. The corresponding revival time exhibits a power law decay with respect to the lattice depth parameter. As far as we are aware, in these two independent quench processes (interaction quench and lattice depth quench), estimation of the timescale of relaxation and revival and their connection with entropy production have not yet been reported. Simulations for a larger number of particles with fixed density produce the same dynamics, demonstrating the generality of our result. Our theoretical investigation of quench dynamics tuning the parameters related to the microscopic Hamiltonian can be verified in future experiments. The immediate open question in this direction is to study how the observed dynamics for contact interaction are affected by the long-range interaction.

Acknowledgments

S Bera wants to acknowledge the Department of Science and Technology (Government of India) for financial support through the INSPIRE fellowship [2015/IF150245]. R Roy acknowledges the UGC fellowship. B Chakrabarti acknowledges FAPESP (grant No. 2016/19622-0) for financial support. BC also acknowledges ICTP support, where a major portion of the work was done. A Gammal acknowledges FAPESP and CNPq for financial support. B Chatterjee acknowledges financial support from the Department of Science and Technology (Government of India) under the DST Inspire Faculty fellowship. We gratefully acknowledge A U J Lode, Prof. G Astrakharchik and M A Garcia-March for some interesting discussions.

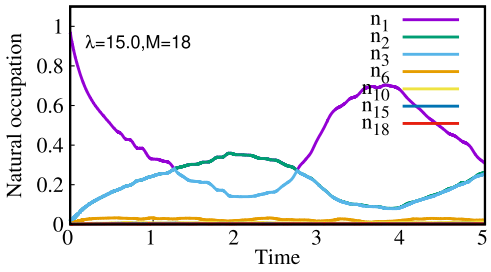

Figure A1. Natural occupations as a function of time for interaction quench to $\lambda = 15.0$, for intermediate time with $N = 3$ bosons in $S = 3$ wells. See text for details. All quantities are dimensionless.

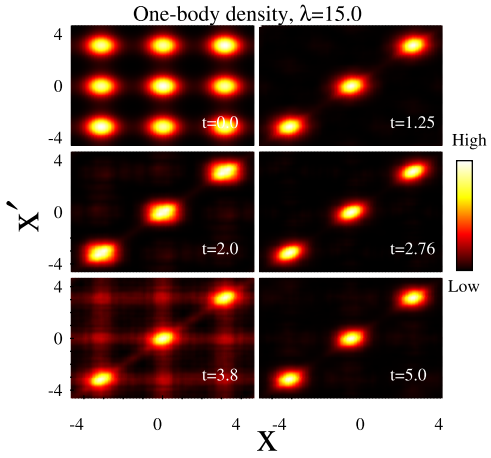

Figure A2. Time evolution of the reduced one-body density matrix $|\rho^{(1)}(x', x)|^2$ for interaction quench $\lambda = 15.0$, for intermediate time with $N = 3$ bosons in $S = 3$ wells. See text for details. All the quantities are dimensionless.

Appendix A. Discussion of the interaction quench for $\lambda = 15.0$ for intermediate time

In this section, we report the evolution of natural occupation and the one-body density matrix for $N = 3$, $S = 3$ for larger time until $t = 5.0$, which is the intermediate timeframe of our simulation. In figure A1, we observe that at $t = 1.25$ the system is close to the fully fragmented *MI* state—the three significantly occupied orbitals have close to 30% population on average. However, from $t = 1.25$ to $t = 2.76$, the n_1, n_2 curves overlap showing identical behavior, while n_3 lowers. In figure A2, we plot the corresponding one-body density matrix. We observe that the system tries to develop some inter-well coherence which is demonstrated by the faded off-diagonal pattern together with the bright diagonal patches. It indicates that the system basically retains its *MI* phase together with very small tunneling between the neighborhood wells. At time $t = 2.76$, we again find the complete extinction of the off-diagonal maxima and 30% occupation of the first three natural orbitals is regained. The system repeats the same dynamics in the timezone $t = 2.76$ to $t = 5.0$. Some off-diagonal correlation is again build up but that cannot be considered as the *SF* phase, and the system passes through the same intermediate phases as reported and finally relaxes to the *MI* phase.

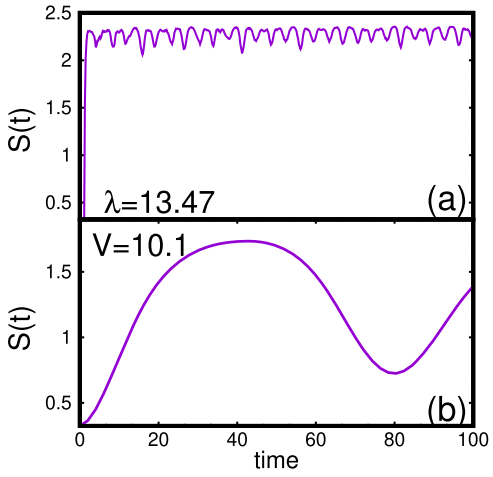

Figure B1. (a) Time evolution of Shannon information entropy $S(t)$ for interaction quench $\lambda = 13.47$ for $N = 5$ bosons in $S = 5$ wells. The sharp linear increase followed by saturation signify that the system relaxes to the maximum entropy state. (b) Time evolution of Shannon information entropy $S(t)$ for lattice-depth quench $V = 10.1$ for $N = 5$ bosons in $S = 5$ wells. The entropy exhibits periodic oscillation and the possibility of relaxation is ruled out. All the quantities are dimensionless.

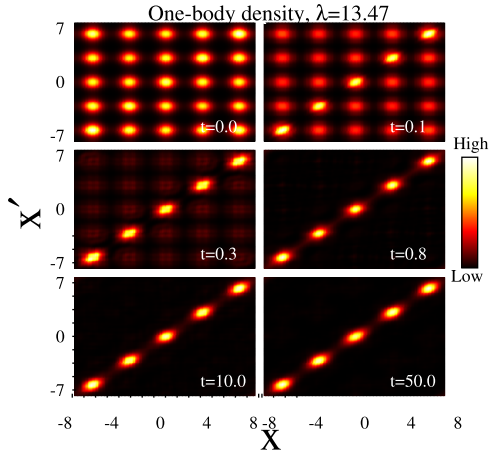

Figure B2. Time evolution of the reduced one-body density matrix $|\rho^{(1)}(x', x)|^2$ for interaction quench $\lambda = 13.47$ for $N = 5$ bosons in $S = 5$ wells. We observe very fast relaxation to *MI* phase (see text). All the quantities are dimensionless.

Appendix B. Relaxation dynamics for $N = 5$ bosons in $S = 5$ wells

We have repeated the calculation for larger lattice and particle numbers keeping the unit filling factor, i.e., $N = 5$ bosons in $S = 5$ wells. To ensure that we are supplying the same amount of excitation energy to both the quench types, we choose $\lambda = 13.47$ for the interaction quench and $V = 10.1$ for the lattice depth quench. Figures B1, B2 and figure B3 summarize our observations which together conclude the same dynamics as reported for $N = 3$ bosons in $S = 3$ wells. For the lattice depth quench we observe identical dynamics (collapse to the *MI* phase and then revival); the revival time also remains unchanged which is also in good agreement with Greiner's experiment. For the interaction quench we also

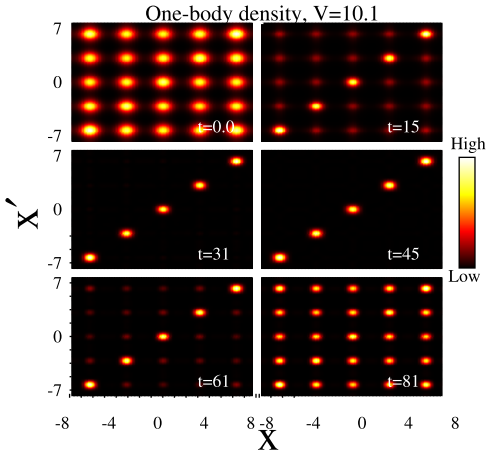

Figure B3. Time evolution of the reduced one-body density matrix $|\rho^{(1)}(x', x)|^2$ for lattice-depth quench $V = 10.1$ for $N = 5$ bosons in $S = 5$ wells. The system exhibits revival in the long time dynamics. All the quantities are dimensionless.

observe fast relaxation to the *MI* phase, only relaxation time is shorter than in the case with $N = 3$ bosons in $S = 3$ wells and $\lambda = 15.0$.

Appendix C. Comparison of *ab initio* results to a Bose–Hubbard model

The Bose–Hubbard model (BHM) is the widely used tool to study weakly interacting bosons in a deep lattice [46–49]. In the BHM, the $SF \rightarrow MI$ transition is determined by the relative strength of the interaction parameter U and the tunneling coupling J. Thus the phase transition is described by a single parameter $\frac{U}{J}$ [46, 50, 51], and $SF \rightarrow MI$ transition can be achieved with high $\frac{U}{J}$ value irrespective of how this ratio is achieved. However, as shown below, the one-to-one correspondence between the BHM parameters and MCTDHB parameters does not hold. So, for the completeness of our present work, we try to construct a bridge between the MCTDHB results, and the findings from the tight-binding approximation.

The triple-well setup can be mapped to a three-site BHM as

$$\hat{H}_{BH} = -J\sum_{i,j} \hat{b}_i^{\dagger}\hat{b}_j + \frac{U}{2}\sum_i \hat{n}_i(\hat{n}_i - 1). \tag{C.1}$$

where U is the on-site interaction parameter and J is the hopping term.

In the tight-binding approximation, the hopping term J is given as

$$J = (4/\sqrt{\pi})E_R(V/E_R)^{3/4}\exp[-2(V/E_R)^{1/2}] \tag{C.2}$$

and the on-site interaction term is given by

$$U = \sqrt{2\pi}(2\lambda/\lambda_0)(V/E_R)^{1/4}, \tag{C.3}$$

$\lambda_0 = 2\pi/k$ [52, 53]. Equations (C.2) and (C.3) basically relate the interaction strength (λ) and lattice depth parameter (V) of our many-body calculation with the hopping term (J) and on-site interaction energy (U) of the BHM. Note that the hopping term J is directly related only to the lattice depth V, but the on-site interaction energy U depends both on the lattice depth V and the two-body interaction λ. Thus for the lattice depth quench (λ fixed), MCTDHB basically corresponds to a simultaneous change in (U, J), whereas the interaction quench (V fixed) corresponds to a quench in U only. Let us summarize the corresponding BHM parameters calculated through equation (C.2) and equation (C.3) for our present many-body calculation.

Table C1. Revival time calculated from entropy dynamics for different combinations of (U, J) and (λ, V) for fixed $\frac{U}{J} = 4.5$.

U	J	λ	V	$t_{revival}$
0.032 1	0.007 1	00216	12.0	372.0
0.020 7	0.004 59	0.013 4	14.0	532.0
0.013 6	0.003	0.008 5	16.0	856.0
0.009	0.002	0.005 6	18.0	1 191.0

For our initial superfluid state with $\lambda = 0.1$ and $V = 3.0$, the corresponding BHM parameters are $J = 0.080\,5$ and $U = 0.105$. For the interaction quench, for the final state with $\lambda = 15.0$ and $V = 3.0$ the corresponding BHM values are $J = 0.080\,5$ and $U = 15.75$. Thus the interaction quench $\lambda = 0.1 \rightarrow \lambda = 15.0$ in our many-body simulation corresponds to the U quench from $U = 0.105 \rightarrow U = 15.75$. For the lattice depth quench, for the final state with $V = 10.1$ and $\lambda = 0.1$ the corresponding BHM values are $U = 0.142$ and $J = 0.011\,1$, thus the lattice depth quench $V = 3.0 \rightarrow V = 10.1$ in our many-body simulation basically corresponds to the change in $J = 0.080\,5 \rightarrow J = 0.011\,1$ and $U = 0.105 \rightarrow U = 0.142$, which does not represent true J quench. Thus an explicit numerical comparison of BHM dynamics with MCTDHB dynamics is beyond the scope of this work. It is to be noted that BHM breaks down for a weak optical lattice as the atoms occupy several vibrational states. In the lowest band approximation, the BHM is valid only when the mean interaction energy per particle is smaller than the energy gap between the lowest two bands. So, the application of BHM is mainly restricted for a weak interaction and deep optical lattice, whereas MCTDHB is accurately applicable for a weak to deep lattice and can address both weakly interacting and strongly interacting bosons in an optical lattice.

In the following paragraph we discuss some interesting aspects of many-body calculation compared to the BHM for a deep lattice where tight-binding approximation works well. We present the entropy dynamics for a fixed $\frac{U}{J} = 4.5$, which addresses the deep lattice physics, and one can investigate the effect of interaction on the timescale of the dynamics. We choose different sets of (U, J), where the choice of each J corresponds to a deep lattice, the corresponding MCTDHB parameters λ and V are further calculated through equations (C.2) and (C.3). For the dynamics, we complete the lattice depth quench; the full set of parameters is presented in table C1. In figure C1, we plot the entropy evolution for

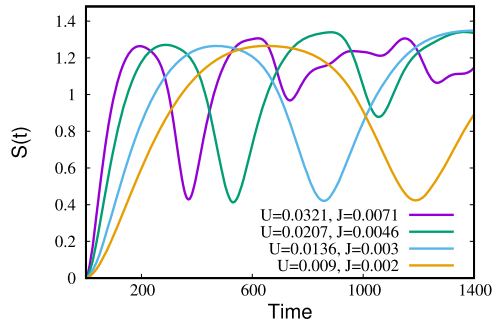

Figure C1. The entropy dynamics for lattice depth quench with fixed $\frac{U}{J} = 4.5$ for several combinations of U and J. See text for details. All the quantities are dimensionless.

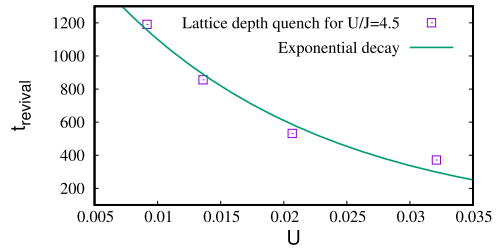

Figure C2. The plot for the revival time for a deep lattice depth quench as a function of the interaction parameter U, which exhibits fast exponential fall as $1\,985.51\,\exp(-59.02\,x)$. See text for details. All the quantities are dimensionless.

different parameter sets; for all cases the revival is observed over quite a long timescale. The smallest J value corresponds to the largest lattice depth V quench and the corresponding revival time is the largest, as expected. However, from the trend in the dynamics, we observe that the amplitude of oscillation in entropy is significantly modified and we expect that eventually the system will relax to a steady state. In figure C2, we plot the corresponding revival time as a function of interaction parameter U. The revival time does exhibit a fast exponential fall, although the magnitude of the fit is understandably different from a pure interaction quench.

In figure C3(a), we show the plot of relaxation time for the interaction quench as a function of $\frac{U}{J}$. The power law with the exponent close to 0.25 is maintained. The variation of revival time for the lattice depth quench with $\frac{U}{J}$ is shown in figure C3(b). There the revival time exhibits a very slow power law decay. The result shows that a pure $\frac{U}{J}$ ratio does not dictate the physics here. Rather, the actual value of the system parameters interaction strength λ and lattice depth V affect the physics.

ORCID iDs

B Chakrabarti https://orcid.org/0000-0002-6320-9894

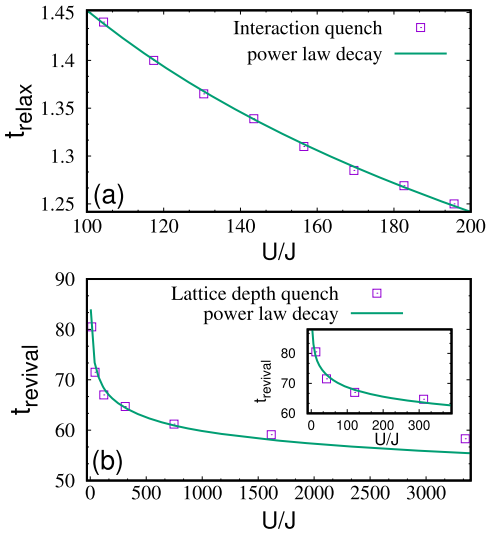

Figure C3. (a) Plot of relaxation time for interaction quench as a function of $\frac{U}{J}$. The curve shows power law decay. The best fit formula is $t_{relax} = 4.11(U/J)^{-0.23}$. (b) Plot for the revival time for lattice depth quench as a function of $\frac{U}{J}$. The best fit formula is $t_{revival} = 92.5(U/J)^{-0.063}$. The variation of $t_{revival}$ for small $\frac{U}{J}$ is presented in the inset. The power law decay remains the same as for large $\frac{U}{J}$. See text for details. All the quantities are dimensionless.

References

[1] Kaufman A M, Tai M E, Lukin A, Rispoli M, Schittko R, Preiss P M and Greiner M 2016 *Science* **353** 794
[2] Trotzky S, Chen Y-A, Flesch A, McCulloch I P, Schollwöck U, Eisert J and Bloch I 2012 *Nat. Phys.* **8** 325
[3] Cheneau M, Barmettler P, Poletti D, Endres M, Schaua P, Fukuhara T, Gross C, Bloch I, Kollath C and Kuhr S 2012 *Nature* **481** 484
[4] Kinoshita T, Wenger T and Weiss D S 2006 *Nature* **440** 900
[5] Greiner M, Mandel O, Esslinger T, Hänsch T W and Bloch I 2002 *Nature* **415** 39
[6] Greiner M, Mandel O, Hänsch T W and Bloch I 2002 *Nature* **419** 51
[7] Will S, Best T, Schneider U, Hackermuller L, Luhmann D and Bloch I 2010 *Nature* **465** 197
[8] Langen T, Geiger R, Kuhnert M, Rauer B and Schmiedmayer J 2013 *Nat Phys* **9** 640
[9] Langen T, Erne S, Geiger R, Rauer B, Schweigler T, Kuhnert M, Rohringer W, Mazets I E, Gasenzer T and Schmiedmayer1 J 2015 *Science* **348** 207
[10] Gring M, Kuhnert M, Langen T, Kitagawa T, Rauer B, Schreitl M, Mazets I, Adu Smith D, Demler E and Schmiedmayer J 2012 *Science* **337** 1318
[11] Collura M, Kormos M and Calabrese P 2018 *Phys. Rev.* A **97** 033609
[12] Minguzzi A and Gangardt D M 2005 *Phys. Rev. Lett.* **94** 240404
[13] Caux J-S and Konik R M 2012 *Phys. Rev. Lett.* **109** 175301
[14] Collura M, Sotiriadis S and Calabrese P 2013 *Phys. Rev. Lett.* **110** 245301
[15] Kormos M, Collura M and Calabrese P 2014 *Phys. Rev.* A **89** 013609
[16] Fagotti M, Collura M, Essler F H L and Calabrese P 2014 *Phys. Rev.* B **89** 125101
[17] Iyer D and Andrei N 2012 *Phys. Rev. Lett.* **109** 115304

[18] Mistakidis S I, Koutentakis G M and Schmelcher P 2018 *Chem. Phys.* **509** 106
[19] Siegl P, Mistakidis S I and Schmelcher P 2018 *Phys. Rev.* A **97** 053626
[20] Neuhaus-Steinmetz J, Mistakidis S I and Schmelcher P 2017 *Phys. Rev.* A **95** 053610
[21] Koutentakis G M, Mistakidis S I and Schmelcher P 2017 *Phys. Rev.* A **95** 013617
[22] Mistakidis S I and Schmelcher P 2017 *Phys. Rev.* A **95** 013625
[23] Bach R and Rzażewski K 2004 *Phys. Rev.* A **70** 063622
[24] Fischer U R and Xiong B 2012 *EPL* **99** 66003
[25] Bernier J S, Roux G and Kollath C 2011 *Phys. Rev. Lett.* **106** 200601
[26] Zakrzewski J and Delande D 2009 *Phys. Rev.* A **80** 013602
[27] Haque M and Zimmer F E 2013 *Phys. Rev.* A **87** 033613
[28] Poletti D and Kollath C 2011 *Phys. Rev.* A **84** 013615
[29] Alon O E, Streltsov A I and Cederbaum L S 2008 *Phys. Rev.* A **77** 033613
[30] Alon O E, Streltsov A I and Cederbaum L S 2007 *J. Chem. Phys.* **127** 154103
[31] Streltsov A I, Alon O E and Cederbaum L S 2007 *Phys. Rev. Lett.* **99** 030402
[32] Olshanii M 1998 *Phys. Rev. Lett.* **81** 938
[33] Fasshauer E and Lode A U J 2016 *Phys. Rev.* A **93** 033635
[34] Lode A U J 2016 *Phys. Rev.* A **93** 063601
[35] Lode A U J, Tsatsos M C, Fasshauer E, Lin R, Papariello L, Molignini P, Lévêque C and Weiner S E 2019 MCTDH-X: The time-dependent multiconfigurational Hartree for indistinguishable particles software (http://ultracold.org)
[36] Mistakidis S I, Cao L and Schmelcher P 2014 *J. Phys. B: At. Mol. Opt. Phys.* **47** 225303
[37] Mistakidis S I, Wulf T, Negretti A and Schmelcher P 2015 *J. Phys. B: At. Mol. Opt. Phys.* **48** 244004
[38] Alon O E, Streltsov A I and Cederbaum L S 2007 *Phys. Rev.* A **76** 013611
[39] Plaßmann T, Mistakidis S I and Schmelcher P 2018 *J. Phys. B: At. Mol. Opt. Phys.* **51** 225001
[40] Mistakidis S I, Cao L and Schmelcher P 2015 *Phys. Rev.* A **91** 033611
[41] Roy R, Gammal A, Tsatsos M C, Chatterjee B, Chakrabarti B and Lode A U J 2018 *Phys. Rev.* A **97** 043625
[42] Nguyen J H V, Tsatsos M C, Luo D, Lode A U J, Telles G D, Bagnato V S and Hulet R G 2019 *Phys. Rev.* X **9** 011052
[43] Lode A U J, Chakrabarti B and Kota V K B 2015 *Phys. Rev.* A **92** 033622
[44] Flambaum V V and Izrailev F M 2001 *Phys. Rev.* E **64** 036220
[45] Berman G P, Borgonovi F, Izrailev F M and Smerzi A 2004 *Phys. Rev. Lett.* **92** 030404
[46] Fisher M P A, Weichman P B, Grinstein G and Fisher D S 1989 *Phys. Rev.* B **40** 546
[47] Sakmann K, Streltsov A I, Alon O E and Cederbaum L S 2009 *Phys. Rev. Lett.* **103** 220601
[48] Fischer U R, Schützhold R and Uhlmann M 2008 *Phys. Rev.* A **77** 043615
[49] Schützhold R, Uhlmann M, Xu Y and Fischer U R 2006 *Phys. Rev. Lett.* **97** 200601
[50] Kühner T D and Monien H 1998 *Phys. Rev.* B **58** R14741
[51] Rapsch S, Schollwöck U and Zwerger W 1999 *Europhys. Lett.* **46** 559
[52] Büchler H P, Blatter G and Zwerger W 2003 *Phys. Rev. Lett.* **90** 130401
[53] Jaksch D *et al* 1998 *Phys. Rev. Lett.* **81** 3108